APEM journal

Advances in Production Engineering & Management **ISSN 1854-6250**
Volume 17 | Number 3 | September 2022 | pp 367–380 Journal home: apem-journal.org
https://doi.org/10.14743/apem2022.3.442 Original scientific paper

Modelling surface roughness in finish turning as a function of cutting tool geometry using the response surface method, Gaussian process regression and decision tree regression

Vukelic, D.[a,*], **Simunovic, K.**[b], **Kanovic, Z.**[a], **Saric, T.**[b], **Doroslovacki, K.**[a], **Prica, M.**[a], **Simunovic, G.**[b]

[a]University of Novi Sad, Faculty of Technical Sciences, Novi Sad, Serbia
[b]University of Slavonski Brod, Mechanical Engineering Faculty in Slavonski Brod, Slavonski Brod, Croatia

ABSTRACT

In this study, the modelling of arithmetical mean roughness after turning of C45 steel was performed. Four parameters of cutting tool geometry were varied, i.e.: corner radius r, approach angle κ, rake angle γ and inclination angle λ. After turning, the arithmetical mean roughness Ra was measured. The obtained values of Ra ranged from 0.13 μm to 4.39 μm. The results of the experiments showed that surface roughness improves with increasing corner radius, increasing approach angle, increasing rake angle, and decreasing inclination angle. Based on the experimental results, models were developed to predict the distribution of the arithmetical mean roughness using the response surface method (RSM), Gaussian process regression with two kernel functions, the sequential exponential function (GPR-SE) and Mattern (GPR-Mat), and decision tree regression (DTR). The maximum percentage errors of the developed models were 3.898 %, 1.192 %, 1.364 %, and 0.960 % for DTR, GPR-SE, GPR-Mat, and RSM, respectively. In the worst case, the maximum absolute errors were 0.106 μm, 0.017 μm, 0.019 μm, and 0.011 μm for DTR, GPR-SE, GPR-Mat, and RSM, respectively. The results and the obtained errors show that the developed models can be successfully used for surface roughness prediction.

ARTICLE INFO

Keywords:
Turning;
Tool geometry;
Modelling;
Surface roughness;
Response surface method;
Decision tree regression;
Gaussian process regression

**Corresponding author:*
vukelic@uns.ac.rs
(Vukelic, D.)

Article history:
Received 13 June 2022
Revised 19 September 2022
Accepted 21 September 2022

1. Introduction

Turning plays an important role in machining. It can be achieved in several ways. The steps that need to be taken must be carefully defined to achieve the desired quality, lower cost and shorter production time. Roughness is an important quality indicator of the machining surface, as it affects the performance of the product, but also the production costs [1]. Numerous factors affect the quality of the machining surface: machining conditions (machine tool rigidity, vibrations, use of cutting fluid, type of cutting fluid, etc.), machining parameters (cutting speed, feed rate and depth of cut), material properties of the workpiece (chemical composition, mechanical properties, physical properties, thermal properties, etc.), and cutting tool parameters (geometry, material, coating, etc.) [2-4]. Cutting tool geometry has a great influence on dimensional accuracy, shape accuracy, tool wear, residual stress, chip shape, cutting force, heat distribution, hardness variation, vibration, and surface roughness.

Various methods have been proposed in the literature that have investigated the effects of tool geometry on surface roughness during turning. For example, Zerti *et al*. [5] studied the effects of corner radius, approach angle, and machining parameters on surface topography. Davoudinejad and Noordin [6] presented the effect of chamfer and honed edge geometry on surface finish. Zhao *et al*. [7] presented the effect of edge radius on surface roughness. Duc *et al*. [8] investigated the effect of cutting edge angle, rake angle, and inclination angle on surface roughness. Neseli *et al*. [9] investigated the influence of corner radius, approach angle and rake angle on surface roughness. Ashish and Lokesha [10] presented the effect of rake angle, approach angle, and process parameters on surface roughness. Karim *et al*. [11] studied the effects of different rake angles on surface roughness. Kumar *et al*. [12] determined the effect of corner radius and approach angle, as well as turning parameters on the surface roughness. Cui *et al*. [13] performed an optimization of corner radius, rake angle and approach angle. Sung *et al*. [14] studied the effect of corner radius micro deviation on surface roughness. Ponugoti *et al*. [15] studied the surface roughness after turning with variable cutting speed, feed, depth of cut, corner radius and negative rake angle. Senthilkumar and Tamizharasan [16] analyzed the influence of insert shape, relief angle, and corner radius on surface roughness. Tauhiduzzaman and Veldhuis [17] investigated the role of tool geometry on roughness using a tool with a rounded primary cutting edge and a flat secondary cutting edge. Abainia and Ouelaa [18] studied the effect of rake angle, approach angle, and inclination angle on surface roughness. Mohammad *et al*. [19] studied the effects of approach angle, rake angle, and inclination angle on surface roughness. Hai *et al*. [20] studied the surface quality with different corner radii, cutting speeds, and feeds. Khellaf *et al*. [21] presented a comparison of surface roughness with coated and uncoated mixed ceramics. Ozdemir [22] investigated the influence of turning parameters and corner radius on surface roughness. Kuntoglu *et al*. [23] investigated the influence of turning parameters and approach angle on surface roughness. In addition, some studies compared the machined surface quality of conventional and wiper inserts after turning operations [24, 25]. The results showed that the wiper insert had better surface roughness performance compared to conventional inserts.

In analyzing the previous research in this field, which investigates the effects of tool geometry on surface roughness, experimental research dominates. The results obtained can only be applied to the conditions under which the experiments were conducted, and the associated cost and time cannot be neglected. To streamline this process, it is possible to model it. Response surface methodology, Taguchi method, artificial neural networks and fuzzy logic are most commonly used to model the turning process [26-28]. Most of the previous research dealt with the effects of machining parameters (cutting speed, feed rate, depth of cut) on the output parameters of the process [29-32].

Soft computing methods were predominantly used for modelling the turning process. When the turning process is properly modelled and the errors in predicting surface roughness are within acceptable limits, the cost and time of experimental investigations are reduced and the subjective influence of the technologist on the results obtained is diminished. There is also greater universality and thus the possibility of practical application. The most important question is which method should be used and when, because each of them has advantages, but also disadvantages. Despite some existing guidelines, it is still not possible to define an algorithm for selecting an appropriate method for specific production conditions. The error between the predicted and experimental values must be within acceptable limits for the prediction model to be used in practice. Finally, the results of all surface roughness prediction methods should converge with increasing accuracy, leading to an integration that accounts for all possible variables. All prediction methods require significant resources to achieve the desired goals. Therefore, it is critical to select an appropriate modelling method and formulate a sufficiently accurate model.

In contrast to previous studies, the objective of this study is to evaluate the influence of four cutting tool geometry parameters, which have not been extensively studied in the literature, on surface roughness. The input parameters were the corner radius r, the approach angle κ, the rake angle γ and the inclination angle λ, while the output parameter was the arithmetical mean roughness Ra. For the obtained results, the modelling of the finish turning was performed with DTR, GPR-SE and GPR-Mat, which were also not previously used for modelling the turning process.

2. Materials and methods

The methodological framework used in the research is shown in Fig. 1. The experimental studies were carried out on a DMG Mori CTX 510 Ecoline CNC lathe. Dry external longitudinal turning was performed on a workpiece with dimensions Ø50 × 600 mm. The workpiece was fixed and clamped by means of the chuck and rotating centre.

The tests were carried out on workpieces made of medium-carbon steel C45, whose chemical composition is 0.42-0.50 % C, 0.50-0.80 % Mn, ≤ 0.4 % Si, ≤ 0.045 % P, ≤ 0.045 % S, ≤ 0.4 % Cr, ≤ 0.4 % Ni, ≤ 0.1 % Mo, and ≤ 0.63 % Cr+Mo+Ni. In addition, the mechanical and physical properties were as follows: density 7.87 g/cm^3, hardness 163 HB, tensile strength 565 MPa, modulus of elasticity 200 GPa, and Poisson's ratio 0.29.

Turning parameters were set for all tests: cutting speed v_c = 440 m/min, feed rate f = 0.10 mm/rev, and depth of cut a_p = 1.5 mm. The parameters were chosen in accordance with the recommendations of the manufacturers of the turning inserts.

CVD-coated (TiCN+Al_2O_3+TiN) turning inserts were used for the experiments. All inserts had the same parameters: effective cutting edge length 10.34 mm, insert thickness 3.175 mm, inscribed circle diameter 6.35 mm, and clearance angle 7°. A new turning insert was used for each experiment. The geometrical parameters of the inserts varied during the experiments are listed in Table 1.

The study was conducted in accordance with the randomized full factorial experiment, which allows the analysis of all combinations of input quantity levels. A total of 3^4 = 81 experiments were performed.

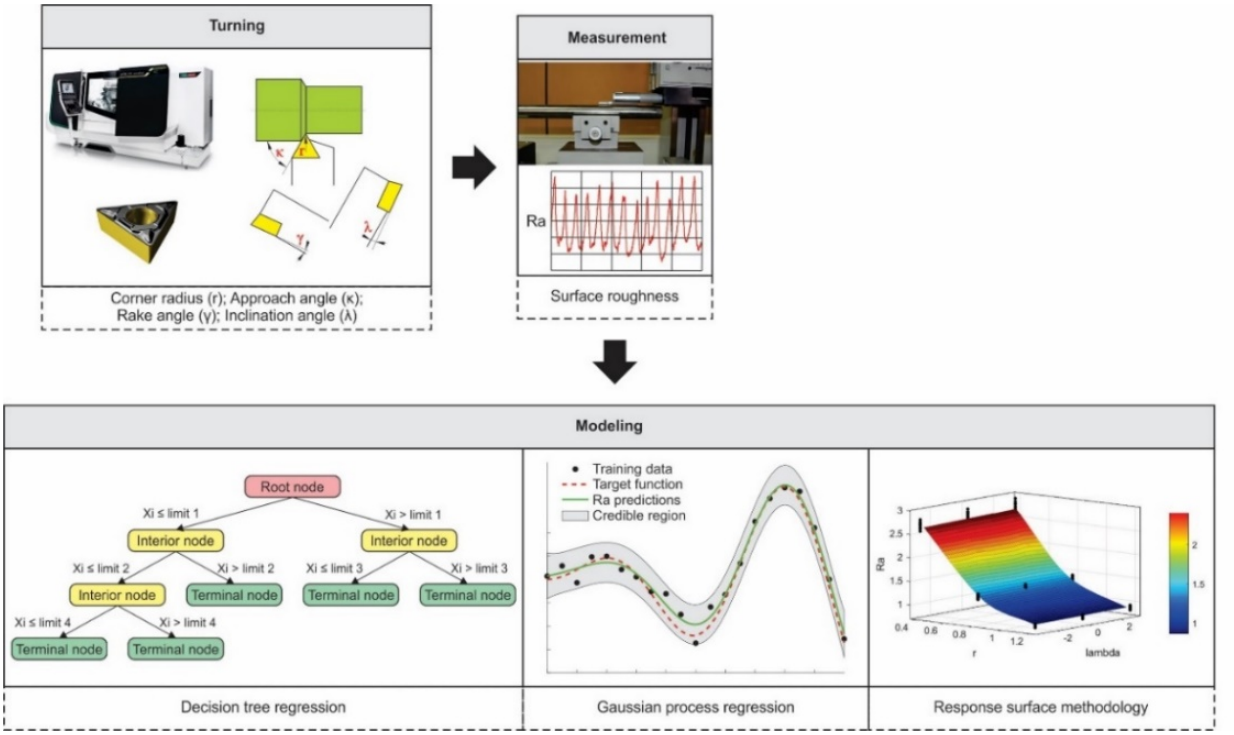

Fig. 1 Methodological framework

Table 1 Turning insert geometry levels (input variables)

Input parameters	Level		
	Low	Medium	High
Corner radius, r (mm)	0.4	0.8	1.2
Approach angle, κ (°)	60	75	90
Rake angle, γ (°)	3	6	9
Inclination angle, λ (°)	-3	0	3

Table 2 Measurement conditions

Parameter	Value
Sampling length	0.8 mm
Cut-off wavelength	0.8 mm
Evaluation length	4 mm
Stylus tip	diamond ball
Stylus radius	2 µm
Stylus force	1 mN

After each experiment, the surface roughness *Ra* was measured. The measurement was performed using a Talysurf 6 measuring instrument, under the conditions listed in Table 2. The surface roughness was measured at six evenly spaced locations along the cut length. The average value from these measurements was taken as the mean value of the surface roughness.

After the experiments were conducted, process modelling was performed based on the obtained results, i.e., prediction of surface roughness with: RSM, DTR, GPR-SE and GPR Mat.

3. Results

3.1 Results of experimental research

The results of experimental research, i.e. the measured values of *Ra* for different combinations of input parameters, are presented in Table 3.

Table 3 Results of experimental research

Run ord.	r (mm)	κ (°)	γ (°)	λ (°)	Ra (μm)	Run ord.	r (mm)	κ (°)	γ (°)	λ (°)	Ra (μm)	Run ord.	r (mm)	κ (°)	γ (°)	λ (°)	Ra (μm)
1	0.8	60	3	-3	1.38	28	0.4	60	6	-3	2.76	55	0.4	60	3	0	2.86
2	0.8	60	6	3	1.39	29	1.2	75	9	0	0.84	56	0.4	75	3	-3	2.74
3	0.4	90	6	3	2.65	30	0.4	60	6	3	2.84	57	1.2	60	9	3	0.88
4	0.4	90	6	-3	2.61	31	1.2	75	9	-3	0.84	58	1.2	75	3	0	0.88
5	1.2	90	9	-3	0.81	32	1.2	90	6	0	0.84	59	0.4	60	6	0	2.80
6	0.8	90	3	3	1.33	33	0.4	90	3	3	2.72	60	0.8	90	9	0	1.27
7	1.2	75	6	0	0.86	34	0.4	90	6	0	2.63	61	0.8	75	9	0	1.30
8	0.8	75	6	0	1.33	35	1.2	90	6	-3	0.83	62	1.2	90	6	3	0.84
9	0.4	90	9	0	2.58	36	0.4	75	6	0	2.71	63	0.8	75	9	3	1.31
10	0.4	60	3	3	2.91	37	1.2	60	9	-3	0.87	64	0.8	75	3	0	1.36
11	0.4	90	9	3	2.60	38	0.8	60	9	-3	1.34	65	1.2	90	9	0	0.82
12	0.4	75	9	-3	2.64	39	1.2	75	6	3	0.87	66	0.8	60	6	0	1.37
13	1.2	75	9	3	0.85	40	1.2	90	3	0	0.86	67	0.8	90	6	0	1.29
14	0.4	90	3	-3	2.68	41	0.8	90	9	-3	1.26	68	1.2	90	3	3	0.86
15	1.2	60	3	0	0.91	42	1.2	60	6	-3	0.87	69	1.2	60	3	3	0.93
16	1.2	60	6	3	0.91	43	1.2	75	3	-3	0.87	70	0.8	90	3	-3	1.31
17	0.4	75	6	-3	2.69	44	0.8	60	6	-3	1.35	71	0.8	60	3	3	1.42
18	0.8	75	9	-3	1.29	45	0.8	90	3	0	1.32	72	1.2	60	9	0	0.87
19	0.8	90	6	-3	1.28	46	0.4	75	9	0	2.66	73	0.8	60	3	0	1.40
20	1.2	90	3	-3	0.85	47	0.8	90	9	3	1.28	74	1.2	90	9	3	0.83
21	0.4	75	3	0	2.77	48	0.8	75	3	3	1.37	75	1.2	60	6	0	0.89
22	0.4	75	3	3	2.80	49	0.8	90	6	3	1.30	76	0.8	75	6	3	1.34
23	0.4	60	9	0	2.75	50	0.4	90	3	0	2.69	77	0.4	60	9	3	2.78
24	1.2	60	3	-3	0.89	51	0.4	75	9	3	2.68	78	0.4	60	3	-3	2.81
25	0.8	60	9	0	1.35	52	0.8	75	6	-3	1.32	79	0.4	90	9	-3	2.56
26	0.8	60	9	3	1.36	53	1.2	75	6	-3	0.85	80	1.2	75	3	3	0.89
27	0.4	75	6	3	2.73	54	0.8	75	3	-3	1.35	81	0.4	60	9	-3	2.72

3.2 Response surface method

The experimental data (Table 3) were statistically processed using Design Expert software (version DX8, 8.0.7.1) and a regression model was derived to predict the surface roughness. Fig. 2 shows the response surface plots of surface roughness resulting from the regression model. Fig. 2 shows that changing the approach angle κ, rake angle γ, and inclination angle λ does not significantly change the surface roughness (Figs. 2a and 2c), while increasing the corner radius r significantly affects the reduction in surface roughness (Figs. 2b and 2d).

Table 4 shows the ANOVA for the reduced quadratic regression model. The nonsignificant interaction terms AD, BC, BD, CD, and the quadratic term A^2 as well as the terms related to interactions between the three factors and higher-order interactions have been removed.

Below is the regression model in terms of the coded (Eq. 1) and the natural (actual) (Eq. 2) input variables.

$$\ln Ra = 0.28 + 0.010 \cdot A - 0.021 \cdot B - 0.031 \cdot C - 0.57 \cdot D - 1.731 \cdot 10^{-3} \cdot A \cdot B - 3.286 \cdot 10^{-3} \cdot A \cdot C + 2.03 \cdot 10^{-3} \cdot B^2 + 2.395 \cdot 10^{-3} \cdot C^2 + 0.14 \cdot D^2 \quad (1)$$

$$\ln Ra = 2.24998 + 0.010042 \cdot \lambda - 9.5811 \cdot 10^{-3} \cdot \gamma - 3.63354 \cdot 10^{-3} \cdot \kappa - 2.82799 \cdot r - 1.92283 \cdot 10^{-4} \cdot \lambda \cdot \gamma - 7.30217 \cdot 10^{-5} \cdot \lambda \cdot \kappa + 2.25531 \cdot 10^{-4} \cdot \gamma^2 + 1.06423 \cdot 10^{-5} \cdot \kappa^2 + 0.87167 \cdot r^2 \quad (2)$$

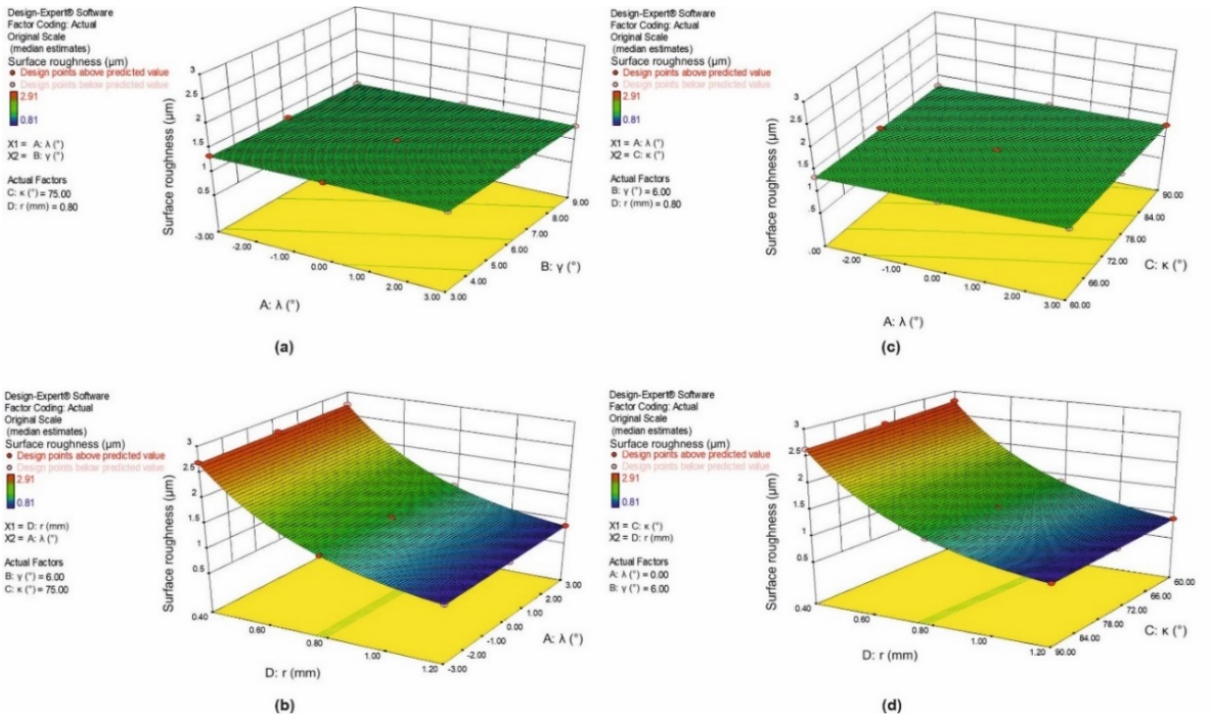

Fig. 2 Response surface plots of surface roughness, a) with approach angle κ and corner radius r at the intermediate levels, b) with rake angle γ and approach angle κ at the intermediate levels, c) with rake angle γ and corner radius r at the intermediate levels, d) with inclination angle λ and rake angle γ at the intermediate levels

Table 4 ANOVA for response surface reduced quadratic model

Source	Sum of Squares	DF	Mean Square	F Value	p-value, Prob > F
Model	18.18	9	2.02	164684.3	< 0.0001
A – inclination angle λ	0.005657	1	0.005657	461.19	< 0.0001
B – rake angle γ	0.023	1	0.023	1872.60	< 0.0001
C – approach angle κ	0.050	1	0.050	4110.92	< 0.0001
D – corner radius r	17.75	1	17.75	1447116	< 0.0001
AB	0.0001078	1	0.0001078	8.79	0.0041
AC	0.0003887	1	0.0003887	31.69	< 0.0001
B^2	7.416 · 10-5	1	7.416 · 10-5	6.05	0.0164
C^2	0.0001032	1	0.0001032	8.41	0.0050
D^2	0.35	1	0.35	28543.75	< 0.0001
Residual	0.0008709	71	1.227 · 10-5		
Cor Total	18.18	80			

Table 5 lists the regression coefficient for each model term, their standard errors, and 95 percent confidence intervals (95 % CI). Confidence intervals are ranges within which the true regression coefficients must fall. In the table, these ranges are low for the intercept, the regression coefficients of A, B, C, D, and D^2, while they are high for AB, AC, B^2, and C^2. However, it is important that the regression coefficients do not span zero, because that would mean that a single regression coefficient can be zero, i.e., that a particular factor has no effect.

Residual analysis follows as an important technique for analyzing regression models. Fig. 3 shows the constructed normal probability plot of the internally studentized residuals to check the assumption of normality of the residuals or errors. From Fig. 3, it can be seen that the error distribution is approximately normal as the graph resembles the straight line. There are small deviations from the straight line at the extremes, but this is not the case for most of the intermediate values. It is also clear that all internally studentized residuals are within ±3 standard deviations from zero (studentized residuals have unit variance), which means that there are no outliers. This is also evident from Fig. 4, which shows the plot of internally studentized residuals against four

factors. Fig. 4 also shows that for the factor D (corner radius *r*), there is some rule for the dependence of the residuals on this factor, i.e. some pattern. Although both positive and negative internally studentized residuals occur (which is fine), there is still smaller scatter for the smaller corner radius and larger for the larger corner radius, which means that it is not a completely constant variance. This is mainly affected by only four internally studentized residuals, i.e., for the experiments labelled 5 and 42 (Run ord.) in Table 3 (the internally studentized residuals are -2.59 and -2.53, respectively) and for experiments 37 and 16 (the internally studentized residuals are 2.68 and 2.95, respectively). These samples were rechecked and it was found that there were no possible errors in the measurement or recording of the results.

Table 5 Standard errors and confidence intervals for regression coefficients

Term	Coefficient Estimate	DF	Standard Error	95 % CI Low	95 % CI High
Intercept	0.28	1	1.030 · 10-3	0.281	0.285
A – inclination angle (λ)	0.010	1	4.766 · 10-4	0.00928	0.011
B – rake angle (γ)	–0.021	1	4.766 · 10-4	–0.0216	–0.01967
C – approach angle (κ)	–0.031	1	4.766 · 10-4	–0.0315	–0.0296
D – corner radius (r)	–0.57	1	4.766 · 10-4	–0.574	–0.572
AB	–1.731 · 10-3	1	5.837 · 10-4	–2.89 · 10-3	–5.67 · 10-4
AC	–3.286 · 10-3	1	5.837 · 10-4	–4.45 · 10-3	–2.12 · 10-3
B^2	2.030 · 10-3	1	8.255 · 10-4	3.84 · 10-4	3.68 · 10-3
C^2	2.395 · 10-3	1	8.255 · 10-4	7.485 · 10-4	4.04 · 10-3
D^2	0.14	1	8.255 · 10-4	0.138	0.141

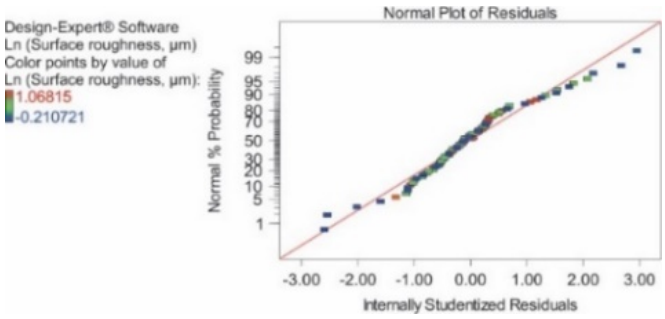

Fig. 3 Normal probability plot of internally studentized residuals

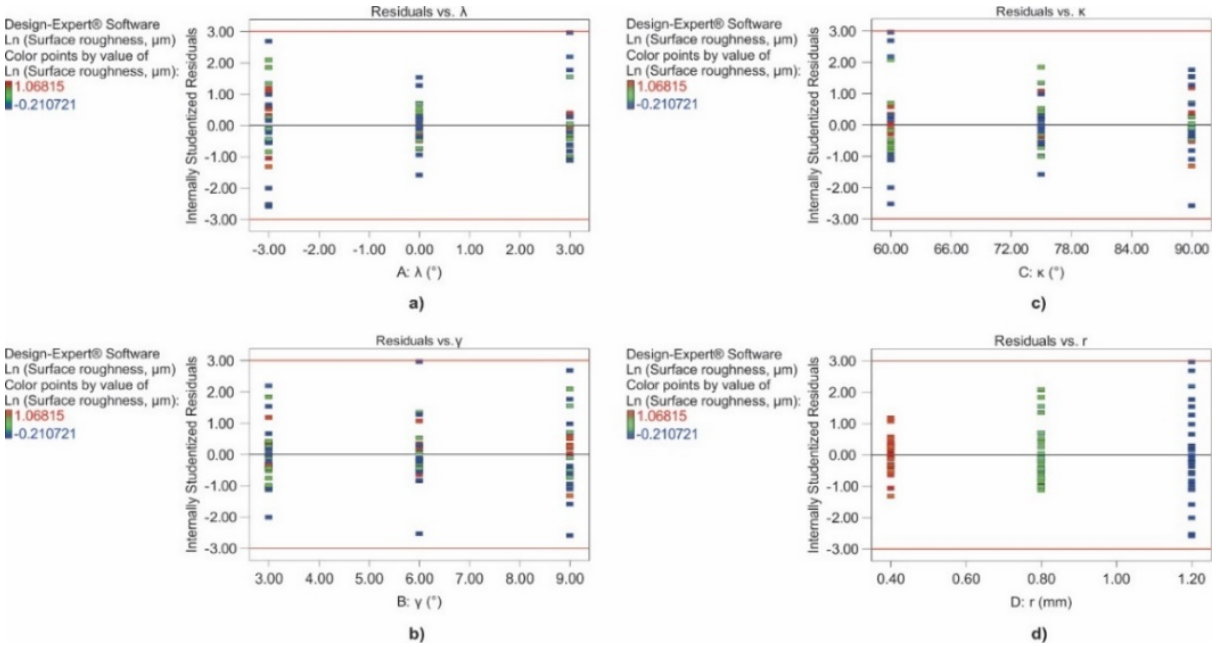

Fig. 4 Residuals versus factors, a) Residuals versus inclination angle λ, b) Residuals versus rake angle γ, c) Residuals versus approach angle κ, d) Residuals versus corner radius r

3.3 Decision tree regression

A decision tree is a machine learning algorithm that can be used for both classification and regression. It is one of the most commonly used practical approaches for supervised learning [33]. In regression, the goal of a decision tree-based model is to predict a continuous output value for a given multivariate input data instance. The model is trained on the given training dataset $\{(x_i, y_i)\}_{i=1}^{N} \in R^m \times R$, where x_i is an m-dimensional input vector and y_i is the corresponding output value. Based on this dataset, a tree-structured regression model is built, as shown in Fig. 1, which consists of three types of nodes. The root node is the initial node which represents the whole dataset. It is split into additional nodes according to the decision (or division) rules contained in both the root node and all subsequent nodes. The interior nodes represent the features of the dataset, and the branches represent the decision (i.e., division) rules. Finally, the leaf nodes represent terminal parts and provide the output results.

The basic idea is to split the entire dataset into groups of "similar" samples, using decision rules contained in interior nodes, applied to input variables x_i [34]. In the decision tree regression problems, the criterion for dataset splitting is the variance of the output value y_i:

$$var = \frac{1}{n}\sum_{1=1}^{n}(y_i - \bar{y})^2 \tag{3}$$

where n is the total number of samples in the node and $\bar{y}$ is the mean of the output values of all samples in the node. Each "parent" node is divided into two "child" nodes. All possible ways of splitting the dataset in a given node are considered, and the one that provides the greatest variance reduction defined as follows:

$$VarRed = var(parent) - \sum_{i=1}^{2} w_i var(child_i) \tag{4}$$

is adopted. In the Eq. 4, w_i is the ratio between the number of elements in the child node and the total number of elements in the parent node. In other words, we split the dataset each time into two new sets, each containing “similar” data, while at the same time the obtained sets differ as much as possible. The described process of node splitting is performed until the desired depth of the tree is reached, which depends on the complexity of the problem.

Once the tree model is trained, it can be used to obtain the predicted value for each new data sample. Following the division rules for the input values x_i, starting from the root node through all the interior nodes, the data sample can be grouped to one of the terminal nodes. The predicted value for that data sample is calculated as the average value of the output values y_i of all the data samples from the training dataset that were grouped to that particular terminal node.

In this study, the following turning process parameters were used as inputs x_1 to x_4: corner radius r, approach angle κ, rake angle γ, and inclination angle λ. The value of the surface roughness Ra was taken as the output parameter y. The tree model was built using Matlab and the application Regression learner, which has three variants for the tree depth according to the maximum number of splits: low, medium and fine tree. All variants were tested, and the fine tree variant, which allows a maximum of 100 splits, was adopted based on the mean square error (MSE) value in the 5-fold cross-validation training procedure. The minimum number of samples per node was set at five, which was determined by a trial-and-error procedure. The cross-validation procedure was also used to remove unnecessary branches to avoid overfitting.

3.4 Gaussian process regression

A Gaussian processes regression is a powerful machine learning technique that can be used to solve a wide variety of supervised learning problems, even when only a small amount of training data is available. It is a probability distribution over possible functions matching a set of points, given with the training dataset $\{(x_i, y_i)\}_{i=1}^{N} \in R^m \times R$, as described previously. The Gaussian process regression is not given in the form of a function, but in a nonparametric form. Thus, instead of computing the probability distribution of the parameters of a specific function, GPR calculates the probability distribution over all admissible functions that fit the data in the dataset.

The regression function modelled by Gaussian process regression has the following form:

$$P(f|X) = \mathcal{N}(f|\mu, K) \tag{5}$$

where $X = [x_1, x_2, \dots, x_N]$, $f = [f(x_1), f(x_2), \dots, f(x_N)]$, $\mu = [m(x_1), m(x_2), \dots, m(x_N)]$ and $K_{ij} = k(x_i, x_j)$. X are the observed input data, m represents the mean function, and K represents a positive definite kernel function, that defines the smoothness of the function, i.e., if the points x_i and x_j are considered similar by the kernel, the function outputs of the two points, $f(x_i)$ and $f(x_j)$ are expected to be similar. Given the points of the training dataset and a mean function f estimated by these points, one can make predictions for each new dataset X_* as $f(X_*)$ with a certain confidence interval depending on the values and distribution of the training dataset. The simple one-dimensional GPR regression is shown in Fig. 1. Based on the training data (black dots), the mean function is determined (green line), and it gives predictions for all new data points X_* with the confidence interval marked in grey.

If we introduce f_* as a prediction for a new dataset X_*, we can express the joint distribution of f and f_* as follows:

$$\begin{bmatrix} f \\ f_* \end{bmatrix} \sim \mathcal{N}\left(\begin{bmatrix} m(X) \\ m(X_*) \end{bmatrix}, \begin{bmatrix} K & K_* \\ K_*^T & K_{**} \end{bmatrix}\right) \tag{6}$$

where $K = K(X, X)$, $K_* = K(X, X_*)$ and $K_{**} = K(X_*, X_*)$. To be able to make a prediction, we need to derive the conditional distribution $P(f_*|f, X, X_*) = \mathcal{N}(f|\mu, K)$. This derivation is given in detail in [35], obtaining:

$$f_*|f, X, X_* \sim \mathcal{N}(K_*^T K\, f, K_{**} - K_*^T K^{-1} K_*) \tag{7}$$

In real applications, however, we do not need exact function values, but rather the noisy version of the data, $y = f(x) + \varepsilon$, where we assume that ε is an additive independent and identically distributed (i.i.d.) Gaussian noise with a variance σ_n^2 that can be determined from the training dataset. The variance function then becomes $\mathrm{cov}(y) = K + \sigma_n^2 I$, and the joint distribution of the observed points (training dataset) and the function values at new dataset points:

$$\begin{bmatrix} y \\ f_* \end{bmatrix} \sim \mathcal{N}\left(\begin{bmatrix} m(X) \\ m(X_*) \end{bmatrix}, \begin{bmatrix} K + \sigma_n^2 \mathrm{I} & K_* \\ K_*^T & K_{**} \end{bmatrix}\right) \tag{8}$$

By deriving the conditional distribution, we get the predictive equations for Gaussian processes regression as follows:

$$\bar{f}_*|y, X, X_* \sim \mathcal{N}\left(\bar{f}_*, \mathrm{cov}(f_*)\right) \tag{9}$$

$$\bar{f}_* \triangleq \mathbb{E}\left[\bar{f}_*|y, X, X_*\right] = K_*^T [K + \sigma_n^2 I]^{-1} y \qquad \mathrm{cov}(f_*) = K_{**} - K_*^T [K + \sigma_n^2 I]^{-1} K_* \tag{10}$$

The practical implementation algorithm for Eqs. 8 to 10 is described in [35]. The best results were obtained with the quadratic exponential kernel (SE) and Matern kernel. The values of kernel parameters were optimized using marginal likelihood as the objective function [35].

3.5 The results of the prediction

Of the total 81 experiments, 72 were used for training and 9 for confirmation. Table 6 shows the results of the training dataset, and Table 7 shows the modelling results of the confirmation dataset. The strength of the modelling, i.e., the deviation between the measured *Ra* value (Ra_{imv}) and the predicted *Ra* value (Ra_{ipv}), was estimated by the absolute error (*AE*) and the percentage error (*PE*) as follows:

$$AE = \left|Ra_{ipv} - Ra_{imv}\right| \tag{11}$$

$$PE = \frac{\left|Ra_{ipv} - Ra_{imv}\right|}{Ra_{imv}} \cdot 100\ \% \tag{12}$$

Table 6 Modelling results of the training dataset

Run ord.	r (mm)	κ (°)	γ (°)	λ (°)	*Ra* (μm)				*PE* (%)				*AE* (μm)			
					DTR	GPR-SE	GPR-Mat	RSM	DTR	GPR-SE	GPR-Mat	RSM	DTR	GPR-SE	GPR-Mat	RSM
1	0.8	60	3	-3	1.368	1.378	1.380	1.382	0.906	0.139	0.025	0.170	0.013	0.002	0.000	0.002
2	0.8	60	6	3	1.368	1.396	1.395	1.391	1.619	0.464	0.391	0.060	0.023	0.006	0.005	0.001
3	0.4	90	6	3	2.625	2.650	2.650	2.651	0.943	0.001	0.004	0.046	0.025	0.000	0.000	0.001
4	0.4	90	6	-3	2.625	2.612	2.613	2.615	0.575	0.077	0.110	0.177	0.015	0.002	0.003	0.005
5	1.2	90	9	-3	0.832	0.812	0.813	0.817	2.675	0.191	0.318	0.835	0.022	0.002	0.003	0.007
6	0.8	90	3	3	1.294	1.328	1.329	1.332	2.726	0.149	0.084	0.142	0.036	0.002	0.001	0.002
7	1.2	75	6	0	0.866	0.859	0.860	0.860	0.698	0.072	0.047	0.039	0.006	0.001	0.000	0.000
8	0.8	75	6	0	1.335	1.327	1.328	1.328	0.376	0.263	0.185	0.175	0.005	0.003	0.002	0.002
9	0.4	90	9	0	2.625	2.581	2.581	2.584	1.744	0.043	0.049	0.168	0.045	0.001	0.001	0.004
10	0.4	60	3	3	2.804	2.906	2.908	2.907	3.651	0.135	0.061	0.107	0.106	0.004	0.002	0.003
11	0.4	90	9	3	2.625	2.600	2.601	2.598	0.962	0.017	0.039	0.082	0.025	0.000	0.001	0.002
13	1.2	75	9	3	0.832	0.848	0.849	0.852	2.157	0.191	0.120	0.200	0.018	0.002	0.001	0.002
14	0.4	90	3	-3	2.625	2.674	2.675	2.670	2.052	0.224	0.180	0.377	0.055	0.006	0.005	0.010
15	1.2	60	3	0	0.894	0.909	0.908	0.910	1.786	0.117	0.171	0.052	0.016	0.001	0.002	0.000
16	1.2	60	6	3	0.894	0.904	0.905	0.901	1.786	0.628	0.543	0.960	0.016	0.006	0.005	0.009
17	0.4	75	6	-3	2.723	2.686	2.687	2.680	1.208	0.139	0.103	0.354	0.033	0.004	0.003	0.010
19	0.8	90	6	-3	1.294	1.281	1.281	1.282	1.074	0.070	0.047	0.146	0.014	0.001	0.001	0.002
20	1.2	90	3	-3	0.848	0.851	0.851	0.848	0.235	0.116	0.062	0.210	0.002	0.001	0.001	0.002
21	0.4	75	3	0	2.723	2.771	2.769	2.770	1.715	0.023	0.024	0.004	0.047	0.001	0.001	0.000
22	0.4	75	3	3	2.723	2.799	2.799	2.803	2.768	0.025	0.027	0.123	0.077	0.001	0.001	0.003
23	0.4	60	9	0	2.804	2.748	2.749	2.747	1.955	0.064	0.043	0.101	0.054	0.002	0.001	0.003
24	1.2	60	3	-3	0.894	0.888	0.889	0.896	0.421	0.229	0.168	0.648	0.004	0.002	0.001	0.006
25	0.8	60	9	0	1.368	1.349	1.348	1.347	1.296	0.105	0.117	0.231	0.017	0.001	0.002	0.003
26	0.8	60	9	3	1.368	1.364	1.363	1.363	0.551	0.286	0.230	0.210	0.007	0.004	0.003	0.003
27	0.4	75	6	3	2.723	2.735	2.733	2.736	0.275	0.181	0.117	0.217	0.007	0.005	0.003	0.006
28	0.4	60	6	-3	2.804	2.760	2.760	2.761	1.585	0.015	0.008	0.043	0.044	0.000	0.000	0.001
29	1.2	75	9	0	0.832	0.843	0.843	0.844	0.992	0.364	0.307	0.534	0.008	0.003	0.003	0.004
30	0.4	60	6	3	2.804	2.837	2.837	2.837	1.276	0.091	0.111	0.110	0.036	0.003	0.003	0.003
31	1.2	75	9	-3	0.832	0.839	0.838	0.837	0.992	0.144	0.215	0.317	0.008	0.001	0.002	0.003
34	0.4	90	6	0	2.625	2.631	2.631	2.633	0.190	0.032	0.028	0.108	0.005	0.001	0.001	0.003
35	1.2	90	6	-3	0.848	0.828	0.829	0.831	2.169	0.220	0.102	0.078	0.018	0.002	0.001	0.001
36	0.4	75	6	0	2.723	2.710	2.709	2.708	0.461	0.001	0.021	0.072	0.013	0.000	0.001	0.002
38	0.8	60	9	-3	1.368	1.338	1.338	1.331	2.052	0.180	0.139	0.665	0.027	0.002	0.002	0.009
39	1.2	75	6	3	0.866	0.867	0.868	0.869	0.460	0.327	0.214	0.093	0.004	0.003	0.002	0.001
40	1.2	90	3	0	0.848	0.856	0.857	0.856	1.395	0.450	0.300	0.511	0.012	0.004	0.003	0.004
41	0.8	90	9	-3	1.294	1.257	1.256	1.260	2.679	0.223	0.349	0.034	0.034	0.003	0.004	0.000
42	1.2	60	6	-3	0.894	0.873	0.871	0.877	2.730	0.313	0.160	0.830	0.024	0.003	0.001	0.007
43	1.2	75	3	-3	0.866	0.871	0.870	0.870	0.460	0.122	0.024	0.048	0.004	0.001	0.000	0.000
44	0.8	60	6	-3	1.368	1.353	1.353	1.354	1.296	0.188	0.203	0.276	0.017	0.003	0.003	0.004
45	0.8	90	3	0	1.294	1.321	1.321	1.320	1.989	0.086	0.073	0.029	0.026	0.001	0.001	0.000
46	0.4	75	9	0	2.723	2.660	2.660	2.658	2.350	0.004	0.007	0.069	0.063	0.000	0.000	0.002
47	0.8	90	9	3	1.294	1.276	1.276	1.274	1.074	0.318	0.306	0.496	0.014	0.004	0.004	0.006
48	0.8	75	3	3	1.335	1.374	1.374	1.374	2.555	0.278	0.283	0.325	0.035	0.004	0.004	0.004
49	0.8	90	6	3	1.294	1.298	1.299	1.300	0.481	0.172	0.103	0.015	0.006	0.002	0.001	0.000
50	0.4	90	3	0	2.625	2.692	2.692	2.693	2.416	0.067	0.062	0.118	0.065	0.002	0.002	0.003
51	0.4	75	9	3	2.723	2.680	2.680	2.681	1.586	0.009	0.007	0.032	0.043	0.000	0.000	0.001
52	0.8	75	6	-3	1.335	1.317	1.318	1.314	1.136	0.240	0.128	0.443	0.015	0.003	0.002	0.006
53	1.2	75	6	-3	0.866	0.852	0.852	0.852	1.882	0.240	0.181	0.185	0.016	0.002	0.002	0.002
54	0.8	75	3	-3	1.335	1.347	1.347	1.342	1.111	0.229	0.206	0.597	0.015	0.003	0.003	0.008
55	0.4	60	3	0	2.804	2.858	2.857	2.863	1.967	0.079	0.101	0.101	0.056	0.002	0.003	0.003
56	0.4	75	3	-3	2.723	2.743	2.743	2.737	0.639	0.109	0.093	0.104	0.018	0.003	0.003	0.003
57	1.2	60	9	3	0.894	0.880	0.881	0.883	1.562	0.009	0.089	0.356	0.014	0.000	0.001	0.003
58	1.2	75	3	0	0.866	0.880	0.880	0.880	1.591	0.012	0.001	0.005	0.014	0.000	0.000	0.000
60	0.8	90	9	0	1.294	1.266	1.267	1.267	1.870	0.344	0.268	0.234	0.024	0.004	0.003	0.003
61	0.8	75	9	0	1.335	1.303	1.303	1.303	2.692	0.202	0.232	0.248	0.035	0.003	0.003	0.003
62	1.2	90	6	3	0.848	0.844	0.843	0.842	0.952	0.520	0.394	0.271	0.008	0.004	0.003	0.002
63	0.8	75	9	3	1.335	1.311	1.311	1.314	1.908	0.068	0.058	0.332	0.025	0.001	0.001	0.004
64	0.8	75	3	0	1.335	1.359	1.359	1.358	1.838	0.054	0.078	0.140	0.025	0.001	0.001	0.002
65	1.2	90	9	0	0.832	0.822	0.822	0.821	1.423	0.203	0.224	0.126	0.012	0.002	0.002	0.001
66	0.8	60	6	0	1.368	1.373	1.371	1.372	0.182	0.192	0.098	0.157	0.003	0.003	0.001	0.002
68	1.2	90	3	3	0.848	0.861	0.860	0.863	1.395	0.074	0.021	0.357	0.012	0.001	0.000	0.003
69	1.2	60	3	3	0.894	0.932	0.931	0.924	3.898	0.210	0.130	0.698	0.036	0.002	0.001	0.006
70	0.8	90	3	-3	1.294	1.315	1.313	1.309	1.240	0.417	0.255	0.078	0.016	0.005	0.003	0.001
72	1.2	60	9	0	0.894	0.870	0.870	0.873	2.730	0.043	0.015	0.319	0.024	0.000	0.000	0.003
73	0.8	60	3	0	1.368	1.406	1.406	1.404	2.321	0.403	0.399	0.257	0.033	0.006	0.006	0.004
74	1.2	90	9	3	0.832	0.832	0.830	0.825	0.201	0.215	0.012	0.563	0.002	0.002	0.000	0.005
75	1.2	60	6	0	0.894	0.887	0.887	0.889	0.421	0.283	0.284	0.095	0.004	0.003	0.003	0.001
76	0.8	75	6	3	1.335	1.338	1.338	1.341	0.373	0.120	0.134	0.100	0.005	0.002	0.002	0.001
77	0.4	60	9	3	2.804	2.778	2.779	2.780	0.854	0.063	0.037	0.007	0.024	0.002	0.001	0.000
78	0.4	60	3	-3	2.804	2.812	2.811	2.820	0.222	0.063	0.047	0.341	0.006	0.002	0.001	0.010
79	0.4	90	9	-3	2.625	2.563	2.562	2.571	2.539	0.108	0.074	0.425	0.065	0.003	0.002	0.011
81	0.4	60	9	-3	2.804	2.721	2.721	2.715	3.079	0.047	0.041	0.183	0.084	0.001	0.001	0.005

Table 7 Modelling results of the confirmation dataset

Run	r (mm)	κ (°)	γ (°)	λ (°)	*Ra* (μm)				*PE* (%)				*AE* (μm)			
					DTR	GPR-SE	GPR-Mat	RSM	DTR	GPR-SE	GPR-Mat	RSM	DTR	GPR-SE	GPR-Mat	RSM
12	0.4	75	9	-3	2.723	2.642	2.642	2.636	3.125	0.065	0.065	0.165	0.083	0.002	0.002	0.004
18	0.8	75	9	-3	1.335	1.297	1.298	1.292	3.488	0.557	0.581	0.169	0.045	0.007	0.008	0.002
32	1.2	90	6	0	0.848	0.837	0.838	0.836	0.952	0.407	0.244	0.423	0.008	0.003	0.002	0.004
33	0.4	90	3	3	2.625	2.710	2.711	2.717	3.493	0.374	0.325	0.123	0.095	0.010	0.009	0.003
37	1.2	60	9	-3	0.894	0.863	0.863	0.863	2.730	0.749	0.859	0.857	0.024	0.007	0.007	0.007
59	0.4	60	6	0	2.804	2.798	2.797	2.799	0.134	0.082	0.121	0.044	0.004	0.002	0.003	0.001
67	0.8	90	6	0	1.294	1.289	1.290	1.291	0.291	0.100	0.025	0.063	0.004	0.001	0.000	0.001
71	0.8	60	3	3	1.368	1.437	1.439	1.425	3.697	1.192	1.364	0.364	0.053	0.017	0.019	0.005
80	1.2	75	3	3	0.866	0.889	0.888	0.891	2.697	0.097	0.186	0.072	0.024	0.001	0.002	0.001

4. Discussion

The descriptive parameters of surface roughness for the experimental tests performed are listed in Table 8. The surface roughness ranges from 0.81 μm to 2.91 μm, with an average value of 1.64 μm and a standard deviation of 0.795 μm. The lowest roughness value ($Ra = Ra_{min}$ = 0.81 μm) was obtained when machining with the largest values for the corner radius ($r = r_{max}$ = 1.2 mm), the largest approach angle ($\kappa = \kappa_{max}$ = 90°), the largest rake angle ($\gamma = \gamma_{max}$ = 9°), and the smallest inclination angle ($\lambda = \lambda_{min}$ = -3°) of the turning insert. The highest roughness value ($Ra = Ra_{max}$ = 2.91 μm) was obtained when machining with the smallest values of corner radius ($r = r_{min}$ = 0.4 mm), the smallest approach angle ($\kappa = \kappa_{min}$ = 60°), the smallest rake angle ($\gamma = \gamma_{min}$ = 3°) and the largest inclination angle ($\lambda = \lambda_{max}$ = 3°) of the turning insert. The ratio values show that the arithmetical mean roughness changes in a wide range for suitable geometrical parameters, which ensures good process control. In other words, the desired quality of the machined surface can be achieved by a suitable choice of input parameters.

The identified trends of the dependence of *Ra* on the input variables are consistent with some previous studies. Feed rate and corner radius have the greatest effect on surface roughness. The roughness of the machined surface decreases (improves) in the following cases: with increasing corner radius [5, 11, 12, 16, 20, 21]; with an increase in positive values of the rake angle [8, 11, 18, 19]; with an increase in the approach angle [5, 8-10, 18], and with the reduction of inclination angle [18], although to varying degrees with different combinations. The results are different, but the trend is identical. Some of the studies also reported the opposite. Surface roughness can also deteriorate (increase) under certain experimental conditions with increasing corner radius [9], smaller approach angle [9, 19], with smaller rake angle [10], and with increasing positive values of inclination angle [19]. Under certain machining conditions, roughness first increases and then decreases with increasing inclination angle [8] and in some cases it first decreases and then increases with increasing inclination angle [12].

Table 8 Descriptive parameters of the surface roughness *Ra*

Parameter	Training *Ra* (μm)	Confirmation *Ra* (μm)
Minimum value	0.810	0.848
Maximum value	2.910	2.804
Mean value	1.637	1.639
Standard deviation	0.795	0.834
Ratio	3.593	3.306

The reduction in roughness at a larger corner radius is a result of the lower and shallower peak height and the lower and shallower valley depth of the machined surface. Higher values of approach angle and positive inclination angle result in lower susceptibility to vibration and thus better quality of the machined surface. Increasing the rake angle improves the sharpness of the cutting edge and thus reduces the roughness of the machined surface. When the approach angle decreases, the contact length of the chip increases, the chip thickness decreases and the chip width increases. The cutting forces are distributed over the longer cutting edge and chip breaking is more difficult. Larger approach angles are characterized by an increase in resistance to auxiliary

movements and a decrease in penetration resistance, as well as a lower tendency to vibration. In the present study, increasing the approach angle resulted in a reduction in roughness, mainly due to minimization of vibration. Reducing the cutting forces reduces the possibility of vibration and thus improving the surface roughness. A negative value of the inclination angle directs chips in the direction of workpiece (in the direction of auxiliary motion) and a positive value directs them in the opposite direction (in the direction opposite to the direction of auxiliary motion). A negative inclination angle increases the cutting edge strength, but also the back force of the cutting resistance, which can lead to chattering. In the present study, negative values of the inclination angle improved surface roughness by increasing cutting edge strength (and reducing the occurrence of various wear mechanisms) and did not affect vibration induction. During turning, the tool tip is exposed to high contact pressures and temperatures in the machining zone, which can increase various wear mechanisms. The smaller corner radius is characterized by lower strength and the larger one by higher strength. The poorest surface finish was obtained with the smallest corner radius. This is due to the low strength of the tool tip and the resulting higher wear rate. The shorter contact length between the tool tip and the workpiece results in less heat dissipation from the shear zone and a higher concentration of heat and stress in this zone. This increases the possibility of tool wear and even thermoplastic deformation of the tool tip.

The visual interpretation of the absolute and percentage errors for all experiments performed (for the training dataset and the confirmation dataset) is shown in Fig. 5, and the minimum, maximum, and mean values for both datasets are shown in Table 9.

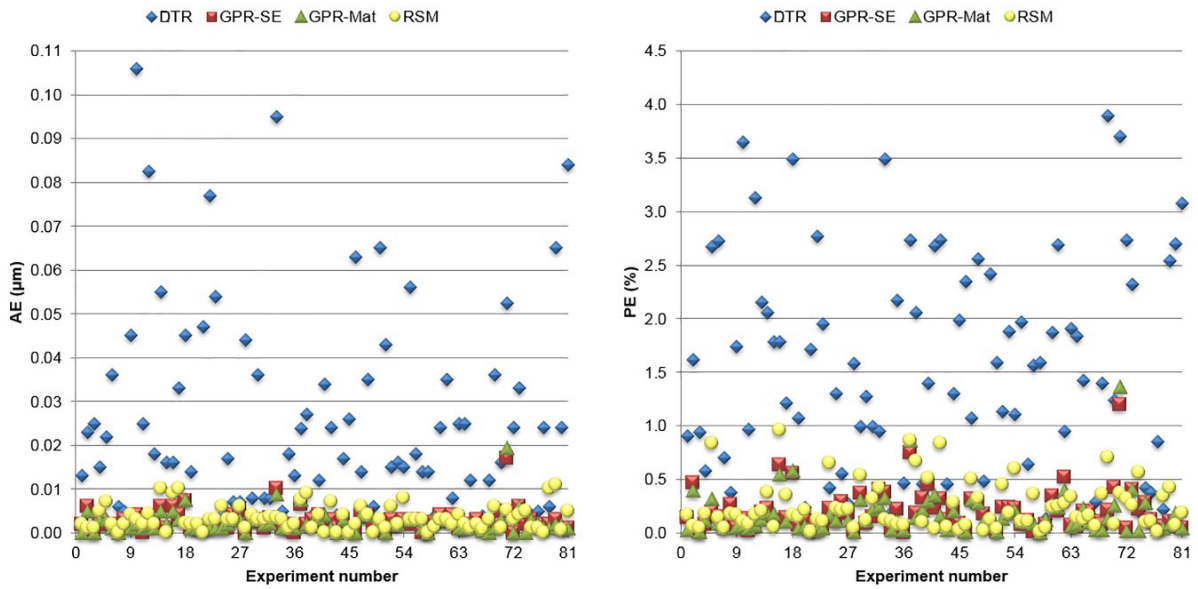

Fig. 5 Visual representation of absolute and percentage errors

Table 9 The percentage and absolute errors of the training and confirmation datasets

Experiment	Value	DTR		GPR-SE		GPR-Mat		RSM	
		PE (%)	*AE* (µm)	*PE* (%)	*AE* (µm)	*PE* (%)	*AE* (µm)	*PE* (%)	*AE* (µm)
Training	Minimum	0.182	0.002	0.001	0.000	0.001	0.000	0.004	0.000
	Maximum	3.898	0.106	0.628	0.006	0.543	0.006	0.960	0.011
	Mean	1.491	0.025	0.168	0.002	0.137	0.002	0.241	0.003
Confirmation	Minimum	0.134	0.004	0.065	0.001	0.025	0.000	0.044	0.001
	Maximum	3.697	0.095	1.192	0.017	1.364	0.019	0.857	0.007
	Mean	2.290	0.038	0.403	0.006	0.419	0.006	0.253	0.003

Based on Fig. 5 and Table 9, the following can be concluded:

- The DTR model had a *PE* of less than 1 % for 28 predictions, a *PE* of between 1% and 2 % for 28 predictions, a *PE* of between 2 % and 3 % for 18 predictions, and a *PE* of between 3 % and

4 % for 7 predictions. The absolute error for all predictions except one (AEmax = 0.106 μm) was less than 0.1 μm. The maximum error values occur during training. The minimum and mean error values also occur during training.

- The model GPR-SE had a *PE* of less than 1 % and an *AE* of less than 0.02 μm (AEmax = 0.017 μm) for all predictions except one (PEmax = 1.192 %). The maximum error values occur at confirmation. The minimum and mean error values occur during training.
- The GPR-Mat model had a *PE* of less than 1 % and an *AE* of less than 0.02 μm (AEmax = 0.019 μm) for all predictions except one (PEmax = 1.364 %). The maximum error values occur at confirmation. The minimum and mean error values occur during training.
- The RSM model had a *PE* of less than 1 % (PEmax = 0.960 %) and an *AE* of less than 0.02 μm (AEmax = 0.011 μm) for all predictions. The maximum error values occur during training. The minimum and average error values also occur during training.

The GPR-SE, GPR-Mat, and RSM models conditionally gave slightly better results, while the DTR model gave slightly worse results. Moreover, the errors in the confirmation experiments are consistent with those of *PE* during the training phase, indicating that the modelling was performed correctly. The extremely low values of the maximum *PE* errors and, most importantly, the correspondingly small values of *AE* (which give a real deviation from the desired value of the surface roughness) show the real possibilities of practical application of all four models in practice.

5. Conclusion

In this study, the integral influence of four parameters of CVD coated cutting tool geometry (corner radius r, approach angle κ, rake angle γ and inclination angle λ on surface roughness of C45 steel workpiece during finish turning was evaluated. Four models were developed based on the experimental results. Confirmation experiments were conducted to validate the model.

The experimental results show that the surface roughness improves with a simultaneous increase in corner radius r, approach angle κ, and rake angle γ, and a decrease in inclination angle λ. The corner radius r has a dominant effect on roughness, followed by the approach angle κ with less effect on surface roughness, the rake angle γ even less and the inclination angle λ with the least.

Based on the experimental results, the modelling of the finish turning process was performed using DTR, GPR-SE, GPR-Mat and RSM. The maximum percentage errors of the developed models were 3.898 %, 1.192 %, 1.364 % and 0.960 % for DTR, GPR-SE, GPR-Mat and RSM, respectively. In the worst case, the maximum absolute errors were 0.106 μm, 0.017 μm, 0.019 μm, and 0.011 μm for DTR, GPR-SE, GPR-Mat, and RSM, respectively. The obtained errors are in the order of tenths and hundredths of micrometers, and in most cases are many times smaller than the allowable processing tolerances in production. Based on the above, all four models can be considered acceptable. Therefore, the developed models can be used in practice as an aid for engineers in selecting the geometrical parameters of the cutting tool during the process planning in order to obtain the required surface roughness.

Future research will focus on studying the influence of various cutting tool geometry factors on surface roughness, inclusion and analysis of other output parameters, and multi-objective optimization of the finish turning process. In addition, future research will consider the other parameters that also affect surface roughness. The integration of a larger number of factors in the model will increase the universality of its application and the accuracy, which is very important in the finish turning, where the influence of all variables is particularly pronounced. One of the future research directions will also be the modelling of surface roughness in finish turning as a function of the geometry of the cutting tool using other methods, as well as the comparison of the results obtained in order to choose the most suitable method for specific machining conditions.

Acknowledgement

This research was funded by the University of Slavonski Brod, Mechanical Engineering Faculty in Slavonski Brod, Republic of Croatia (grant number SV001) and by the Ministry of Education, Science and Technological Development of Republic of Serbia (grant number 451-03-68/2022-14/200156).

References

[1] Kramar, D., Cica, D. (2021). Modeling and optimization of finish diamond turning of spherical surfaces based on response surface methodology and cuckoo search algorithm, *Advances in Production Engineering & Management*, Vol. 16, No. 3, 326-334, doi: 10.14743/apem2021.3.403.

[2] Sterpin Valic, G., Cukor, G., Jurkovic, Z., Brezocnik, M. (2019). Multi-criteria optimization of turning of martensitic stainless steel for sustainability, *International Journal of Simulation Modelling*, Vol. 18, No. 4, 632-642, doi: 10.2507/IJSIMM18(4)495.

[3] Ratnam, M.M. (2017). 1.1 Factors affecting surface roughness in finish turning, In: Hashmi, M.S.J. (ed.), *Comprehensive materials finishing*, Elsevier, Oxford, United Kingdom, 1-25, doi: 10.1016/B978-0-12-803581-8.09147-5.

[4] Kang, W.T., Derani, M.N., Ratnam, M.M. (2020). Effect of vibration on surface roughness in finish turning: Simulation study, *International Journal of Simulation Modelling*, Vol. 19, No. 4, 595-606, doi: 10.2507/IJSIMM19-4-531.

[5] Zerti, O., Yallese, M.A., Khettabi, R., Chaoui, K., Mabrouki, T. (2017). Design optimization for minimum technological parameters when dry turning of AISI D3 steel using Taguchi method, *International Journal of Advanced Manufacturing Technology*, Vol. 89, 1915-1934, doi: 10.1007/s00170-016-9162-7.

[6] Davoudinejad, A., Noordin, M.Y. (2014). Effect of cutting edge preparation on tool performance in hard-turning of DF-3 tool steel with ceramic tools, *Journal of Mechanical Science and Technology*, Vol. 28, 4727-4736, doi: 10.1007/s12206-014-1039-9.

[7] Zhao, T., Zhou, J.M., Bushlya, V., Ståhl, J.E. (2017). Effect of cutting edge radius on surface roughness and tool wear in hard turning of AISI 52100 steel, *International Journal of Advanced Manufacturing Technology*, Vol. 91, 3611-3618, doi: 10.1007/s00170-017-0065-z.

[8] Duc, P.M., Giang, L.H., Dai, M.D., Sy, D.T. (2020). An experimental study on the effect of tool geometry on tool wear and surface roughness in hard turning, *Advances in Mechanical Engineering*, Vol. 12, No. 9, 1-11, doi: 10.1177/1687814020959885.

[9] Neşeli, S., Yaldız, S., Türkeş, E. (2011). Optimization of tool geometry parameters for turning operations based on the response surface methodology, *Measurement*, Vol. 44, No. 3, 580-587, doi: 10.1016/j.measurement.2010.11.018.

[10] Ashish George, J., Lokesha, K. (2019). Optimisation and effect of tool rake and approach angle on surface roughness and cutting tool vibration, *SN Applied Sciences*, Vol. 1, Article No. 1133, doi: 10.1007/s42452-019-1175-z.

[11] Karim, Z., Azuan, S.A.S., Yasir, A. (2013). A study on tool wear and surface finish by applying positive and negative rake angle during machining, *Australian Journal of Basic and Applied Sciences*, Vol. 7, No. 10, 46-51.

[12] Kumar, S., Singh, D., Kalsi, N.S. (2019). Investigating the effect of approach angle and nose radius on surface quality of Inconel 718, *Journal of The Institution of Engineers (India): Series C*, Vol. 100, 121-128, doi: 10.1007/s40032-017-0411-9.

[13] Cui, X., Guo, J., Zheng, J. (2016). Optimization of geometry parameters for ceramic cutting tools in intermittent turning of hardened steel, *Materials & Design*, Vol. 92, 424-437, doi: 10.1016/j.matdes.2015.12.089.

[14] Sung, A.N., Loh, W.P., Ratnam, M.M. (2016). Simulation approach for surface roughness interval prediction in finish turning, *International Journal of Simulation Modelling*, Vol. 15, No. 1, 42-55, doi: 10.2507/IJSIMM15(1)4.320.

[15] Ponugoti, U., Dantuluri, R.R., Koka, N.S.S., Bhuvanagiri, R.S. (2020). Experimental investigations on the influence of cutting and tool geometry parameters over the machinability of AISI 52100 steel in hard turning, *International Journal of Modern Manufacturing Technologies*, Vol. 12, No. 1, 144-156.

[16] Senthilkumar, N., Tamizharasan, T. (2014). Effect of tool geometry in turning AISI 1045 steel: experimental investigation and FEM analysis, *Arabian Journal for Science and Engineering*, Vol. 39, 4963-4975, doi: 10.1007/s13369-014-1054-2.

[17] Tauhiduzzaman, M., Veldhuis, S.C. (2014). Effect of material microstructure and tool geometry on surface generation in single point diamond turning, *Precision Engineering*, Vol. 38, No. 3, 481-491, doi: 10.1016/j.precisioneng.2014.01.002.

[18] Abainia, S., Ouelaa, N. (2015). Experimental study of the combined influence of the tool geometry parameters on the cutting forces and tool vibrations, *International Journal of Advanced Manufacturing Technology*, Vol. 79, 1127-1138, doi: 10.1007/s00170-015-6885-9.

[19] Mohammad, R., Ariffin, M.K.A.M., Baharuddin, B.T.H.T., Mustapha, F., Aoyama, H. (2017). The effects of single cutting tool geometry on surface roughness, *Journal of Mechanical Engineering*, Vol. 3, No. 1, 45-54.

[20] Hai, S., Jung, H.-C., Shim, W.-H., Shin, H.-G. (2021). Investigation of surface quality for minor scale diameter of biodegradable magnesium alloys during the turning process using a different tool nose radius, *Metals*, Vol. 11, No. 8, Article No. 1174, doi: 10.3390/met11081174.

[21] Khellaf, A., Aouici, H., Smaiah, S., Boutabba, S., Yallese, M.A., Elbah, M. (2017). Comparative assessment of two ceramic cutting tools on surface roughness in hard turning of AISI H11 steel: Including 2D and 3D surface topography, *International Journal of Advanced Manufacturing Technology*, Vol. 89, 333-354, doi: 10.1007/s00170-016-9077-3.

[22] Özdemir, M. (2020). Modelling and prediction of effect of machining parameters on surface roughness in turning operations, *Tehnički Vjesnik – Technical Gazette,* Vol. 27, No. 3, 751-760, doi: 10.17559/TV-20190320104114.
[23] Kuntoğlu, M., Aslan, A., Pimenov, D.Y., Giasin, K., Mikolajczyk, T., Sharma, S. (2020). Modeling of cutting parameters and tool geometry for multi-criteria optimization of surface roughness and vibration via response surface methodology in turning of AISI 5140 steel, *Materials*, Vol. 13, No. 19, Article No. 4242, doi: 10.3390/ma13194242.
[24] Šarić, T., Vukelić, D., Šimunović, K., Svalina, I., Tadić, B., Prica, M., Šimunović, G. (2020). Modelling and prediction of surface roughness in CNC turning process using neural networks, *Tehnički Vjesnik – Technical Gazette,* Vol. 27, No. 6, 1923-1930, doi: 10.17559/TV-20200818114207.
[25] Zhang, P., Liu, Z. (2016). Modeling and prediction for 3D surface topography in finish turning with conventional and wiper inserts, *Measurement*, Vol. 94, 37-45, doi: 10.1016/j.measurement.2016.07.080.
[26] Benardos, P.G., Vosniakos, G.-C. (2003). Predicting surface roughness in machining: A review, *International Journal of Machine Tools and Manufacture*, Vol. 43, No. 8, 833-844, doi: 10.1016/S0890-6955(03)00059-2.
[27] Sousa, V.F.C., Silva, F.J.G. (2020). Recent advances in turning processes using coated tools –A comprehensive review, *Metals*, Vol. 10, No. 2, Article No. 170, doi: 10.3390/met10020170.
[28] Dureja, J.S., Gupta, V.K., Sharma, V.S., Dogra, M., Bhatti, M.S. (2016). A review of empirical modeling techniques to optimize machining parameters for hard turning applications, *Proceedings of the Institution of Mechanical Engineers, Part B: Journal of Engineering Manufacture*, Vol. 230, No. 3, 389-404, doi: 10.1177/0954405414558731.
[29] He, C.L., Zong, W.J., Zhang, J.J. (2018). Influencing factors and theoretical modeling methods of surface roughness in turning process: State-of-the-art, *International Journal of Machine Tools and Manufacture*, Vol. 129, 15-26, doi: 10.1016/j.ijmachtools.2018.02.001.
[30] Puh, F., Jurkovic, Z., Perinic, M., Brezocnik, M., Buljan, S. (2016). Optimization of machining parameters for turning operation with multiple quality characteristics using Grey relational analysis, *Tehnički Vjesnik – Technical Gazette,* Vol. 23, No. 2, 377-382, doi: 10.17559/TV-20150526131717.
[31] Trung, D.D., Thinh, H.X. (2021). A multi-criteria decision-making in turning process using the MAIRCA, EAMR, MARCOS and TOPSIS methods: A comparative study, *Advances in Production Engineering & Management*, Vol. 16, No. 4, 443-456, doi: 10.14743/apem2021.4.412.
[32] Savićević, S., Vukćević, M., Klimenko, S.A., Tanović, L. (2017). Impact of cutting elements on forces and roughness of surface during turning hard steel X160 CrMo V12 with CBN tool, *Tehnički Vjesnik – Technical Gazette,* Vol. 24, No. 4, 1001-1006, doi: 10.17559/TV-20161013100743.
[33] Ortuño, F.M., Valenzuela, O., Prieto, B., Saez-Lara, M.J., Torres, C., Pomares, H., Rojas, I. (2015). Comparing different machine learning and mathematical regression models to evaluate multiple sequence alignments, *Neurocomputing*, Vol. 164, 123-136, doi: 10.1016/j.neucom.2015.01.080.
[34] Breiman, L., Friedman, J., Olshen, R.A., Stone, C.J (1984). *Classification and regression trees*, First edition, CRC Press, Boca Raton, Florida, USA, doi: 10.1201/9781315139470.
[35] Rasmussen, C.E., Williams, C.K.I. (2006). *Gaussian processes for machine learning*, MIT Press, Cambridge, United Kingdom, doi: 10.7551/mitpress/3206.001.0001.